AGU PUBLICATIONS

Geochemistry, Geophysics, Geosystems

RESEARCH ARTICLE
10.1002/2014GC005343

Key Points:
- Distinct magnetic groups are identified in ocean crust in ODP/IODP Hole 1256D
- Multivariate statistics on magnetic properties complements electrofacies data
- Only specific portions of ocean crust can provide meaningful paleointensity

Supporting Information:
- Readme
- Supporting information

Correspondence to:
M. J. Dekkers,
m.j.dekkers@uu.nl

Citation:
Dekkers, M. J., D. Heslop, E. Herrero-Bervera, G. Acton, and D. Krasa (2014), Insights into magmatic processes and hydrothermal alteration of in situ superfast spreading ocean crust at ODP/IODP site 1256 from a cluster analysis of rock magnetic properties, *Geochem. Geophys. Geosyst.*, *15*, 3430–3447, doi:10.1002/2014GC005343.

Received 17 MAR 2014
Accepted 13 JUL 2014
Accepted article online 16 JUL 2014
Published online 22 AUG 2014

Insights into magmatic processes and hydrothermal alteration of in situ superfast spreading ocean crust at ODP/IODP site 1256 from a cluster analysis of rock magnetic properties

Mark J. Dekkers[1,2,3], David Heslop[2], Emilio Herrero-Bervera[3], Gary Acton[4], and David Krasa[3,5,6]

[1]Paleomagnetic Laboratory "Fort Hoofddijk," Faculty of Geosciences, Utrecht University, Utrecht, Netherlands, [2]Research School of Earth Sciences, Australian National University, Canberra, Australia, [3]HGIP, University of Hawaii at Manoa, Honolulu, Hawaii, USA, [4]Department of Geography and Geology, Sam Houston State University, Huntsville, Texas, USA, [5]School of Geosciences, University of Edinburgh, Edinburg, UK, [6]Now at ERC, Brussels, Belgium

Abstract We analyze magnetic properties from Ocean Drilling Program (ODP)/Integrated ODP (IODP) Hole 1256D (6°44.1′ N, 91°56.1′ W) on the Cocos Plate in ~15.2 Ma oceanic crust generated by superfast seafloor spreading, the only drill hole that has sampled all three oceanic crust layers in a tectonically undisturbed setting. Fuzzy c-means cluster analysis and nonlinear mapping are utilized to study down-hole trends in the ratio of the saturation remanent magnetization and the saturation magnetization, the coercive force, the ratio of the remanent coercive force and coercive force, the low-field magnetic susceptibility, and the Curie temperature, to evaluate the effects of magmatic and hydrothermal processes on magnetic properties. A statistically robust five cluster solution separates the data predominantly into three clusters that express increasing hydrothermal alteration of the lavas, which differ from two distinct clusters mainly representing the dikes and gabbros. Extensive alteration can obliterate magnetic property differences between lavas, dikes, and gabbros. The imprint of thermochemical alteration on the iron-titanium oxides is only partially related to the porosity of the rocks. Thus, the analysis complements interpretation based on electrofacies analysis. All clusters display rock magnetic characteristics compatible with an ability to retain a stable natural remanent magnetization suggesting that the entire sampled sequence of ocean crust can contribute to marine magnetic anomalies. Paleointensity determination is difficult because of the propensity of oxyexsolution during laboratory heating and/or the presence of intergrowths. The upper part of the extrusive sequence, the granoblastic dikes, and moderately altered gabbros may contain a comparatively uncontaminated thermoremanent magnetization.

1. Introduction

The issue of the source of the marine magnetic anomalies or "stripes" is not resolved despite considerable research effort [e.g., *Harrison*, 1987; *Raymond and Labrecque*, 1987; *Pariso and Johnson*, 1993; *Tivey*, 1996; *Gee and Kent*, 2007]. The inherent nonuniqueness of potential methods precludes the determination of the intensity and thickness of the magnetized layer at the same time [e.g., *Blakely*, 1995]. Underneath a sediment layer of variable thickness, oceanic crust is typified by the well-known sequence of a topmost pile of extrusive lava flows, underlain by subvertical sheeted feeder dikes, commonly referred to as the sheeted-dike complex, which is in turn underlain by gabbroic rocks. The upper crust consists of these extrusives and sheeted dikes while the gabbroic part is isotropic and coarse-grained. More evolved gabbro units are often intruded into less evolved units. In the lower crust, the gabbros are foliated and layered [e.g., *France et al.*, 2009].

While the topmost ocean floor lavas are comparatively easy to sample and study, deeper segments of oceanic crust can only be sampled in fortuitous tectonic circumstances, such as, when gabbros and underlying ultramafic mantle rock are juxtaposed with higher-level crustal rocks through extensional detachments as oceanic core complexes [e.g., *Dick et al.*, 2000; *Suhr et al.*, 2008]. Alternative options to expose dikes are escarpments, like in the Hess Deep Rift [e.g., *Francheteau et al.*, 1990], and scarps along transform faults [e.g., *Tivey*, 1996]. Also relatively unaltered obducted oceanic ophiolite crust occurs in Oman and on Cyprus where it has been extensively studied by a variety of techniques [e.g., *Lamoureux et al.*, 1999; *Gillis*, 2002, 2008; *Nicolas et al.*, 2008].

Naturally, questions arise to whether the easily accessible but tectonically disturbed fragments of oceanic crust are representative of the overall oceanic crust. These concerns can be alleviated by sampling undisturbed oceanic crust, such as generated by parts of ridges well away from fracture zones or other discontinuities due to ridge segmentation or propagation. Such representative locations are necessary for understanding the dike/gabbro transition and interaction [e.g., *Nicolas et al*., 2008], but can only be accessed by drilling. The selection of an accessible site where all the primary layers of oceanic crust can be penetrated, is determined by both seafloor spreading processes and technical drilling limitations: the depth to the melt-lens reflector and hence to the gabbros diminishes with increasing spreading rate [*Phipps Morgan and Chen*, 1993] and penetrating basement deeper than 1.5–2 km is technically challenging. Therefore, as outlined by *Wilson et al*. [2003, 2006], Site 1256 was selected, because it resides in crust created by superfast spreading. This makes it possible to reach the gabbro layer by drilling shallower than at Site 504B or other sites in slow- or intermediate-spreading crust. Indeed, this proved to be the case for Hole 1256D, where drilling succeeded in reaching the top of the gabbros [*Wilson et al*., 2006]. *France et al*. [2009] further suggested that the bottom of Hole 1256D penetrates just through the transition from dikes to the foliated gabbros and therefore represents the top of the (fossilized) melt lens. Thus, Site 1256 is currently the only place on Earth where all the primary layers of an in situ section of oceanic crust have been sampled.

The interplay of magmatic and hydrothermal alteration processes and their effects on magnetic mineralogy can thus be evaluated in an undisturbed setting throughout the entire upper ocean crust. To evaluate this interplay, we use fuzzy c-means cluster analysis (FCM) on a set of mineral-magnetic parameters. FCM is a multivariate statistical approach that enables unsupervised partitioning of samples into groups that can subsequently be interpreted [e.g., *Höppner et al*., 1999]. Through the calculation of how similar a case (or sample) is to all clusters, fuzzy clustering techniques allow consideration of gradual boundaries in multivariate data sets, the rule in nature. They are often preferred over classical hierarchical clustering techniques. Here, we interpret changes in mineral magnetic properties categorized in clusters in terms of magmatic and hydrothermal alteration and subsequently discuss implications for paleointensity determination and how the magnetizability of various portions of the ocean crust provides constraints on their contribution to marine magnetic anomalies.

2. Concise Geological and Mineralogical Description of IODP Hole 1256D

Here, we focus on the rock description of Hole 1256D drilled during ODP Leg 206 [*Wilson et al*., 2003] and IODP Expeditions 309 and 312 [*Teagle et al*., 2006]. Below the sediment cover, the extrusive section (250–1061 meters below seafloor (mbsf)) consists of about 25 m of basalts that cap a ~75 m thick lava pond, which is underlain by ~185 m of inflated flows, ~470 m of sheeted and massive flows, and then a ~55 m thick transition zone before the sheeted dikes are entered. The sheeted dike complex is ~346 m thick (1061–1407 mbsf) and is underlain by a plutonic gabbro zone that extends down to the base of the hole at 1507.1 mbsf.

The lava pond is interpreted to be the result of off-axis eruptive activity because the paleomagnetic direction of the lava is anomalously steep for an equatorial site, suggesting it was erupted during a polarity transition and Site 1256 lies ~5 km east of the Anomaly 5Bn-5Br transition [*Wilson et al*., 2003]. Additionally, in nearby Hole 1256C, some sediment is found between the inflated flows and the pond itself [*Wilson et al*., 2003]. Lavas directly underlying the lava pond contain subvertical hyaloclastite-filled inflation structures, indicating eruption onto a near-horizontal surface. Contacts between units in the lava pond are mainly horizontal as well. They become steeper downhole toward the sheeted dike complex [*Tartarotti et al*., 2009].

The lithologic transition zone between the lavas and the sheeted dikes is characterized by the first subvertical igneous contacts and mineralized breccias. It coincides with a stepwise increase in alteration grade: low-temperature clay minerals and oxyhydroxides ($<150^{\circ}$C) are alteration products in the lavas while chlorite and other greenschist facies minerals occur in the sheeted dikes ($>250^{\circ}$C) [*Wilson et al*., 2006; *Teagle et al*., 2006]. The sheeted dikes themselves comprise massive basalt and dolerite with common subvertical chilled margins. Thin dikes intruded in water-filled cracks with quenching and associated hydrofracturing as a result.

The plutonic section comprises two gabbroic intervals, which are 52 and 24 m thick, that intruded a 24 m thick intervening interval, referred to as the dike screen (1458.9–1483.1 mbsf), which is granoblastically

recrystallized [*Teagle et al*., 2006]. The gabbro rocks sampled are similar in chemistry to the overlying dikes [*Wilson et al*., 2006]. The magnesium numbers (Mg#s) of secondary clinopyroxenes are lower than those of primary clinopyroxenes. Bulk rock Mg# does not change [*Teagle et al*., 2006] so the iron is contained in secondary magnetite, likely explaining the widespread occurrence of very fine-grained opaques in altered clinopyroxene. The dike-gabbro transition is the boundary between the active magma system with its melt lens and the lower-temperature convecting hydrothermal system in the sheeted dikes and above.

After having been cooled substantially by hydrothermal action, the lowest ~60 m of the sheeted dikes were transformed to granoblastic dikes under granulite facies conditions [*Koepke et al*., 2008], forming in the so-called "dry" domains. A heat source beneath induced the prograde metamorphism. The two-pyroxene thermometer [*Andersen et al*., 1993] indicates a temperature range of 940–1050°C for the peak conditions. The heat source must have provided the thermal energy for several thousands of years as modeled by *Koepke et al*. [2008]. Most likely, it involved an axial magma chamber located near the base of the sheeted dikes. Later, "wet" domains formed under amphibolite facies in a temperature regime between 700 and 850°C as indicated by the amphibole-plagioclase thermometer [*Holland and Blundy*, 1994]. The oxides continued to equilibrate down to temperatures of 540–600°C as inferred from the two-oxide geothermometer [*Sauerzapf et al*., 2008], which was considerably lower than peak metamorphic conditions. The thermometers show increasing temperature with depth in line with a heat source below the sheeted dikes. Oxides occur as coarse lamellar intergrowths of magnetite/hemoilmenite solid solutions and rare large magnetite grains with significantly different compositions from the titanomagnetite that occurs in the "fresh" lavas and dikes [*Koepke et al*., 2008; *Krása et al*., 2011]. The degree of oxidation parameter z for titanomagnetite (unoxidized titanomagnetite has $z = 0$, completely oxidized or maghemitized titanomagnetite has $z = 1$) is consistently <0.2 for the lowermost dike section (the granoblastic dikes; 1348–1407 mbsf) and gabbros, whereas $z \approx 0.6$ for all the igneous section above 1348 mbsf [*Krása et al*., 2011]. The oxides in this interval also have low ulvöspinel content (8–18 mol % versus 61–74 mol %) and low Al_2O_3 contents (0.4–0.9 versus 0.9–2.3 wt%) [*Dziony et al*., 2008]. The composition is reset to the ambient temperature and redox conditions during granoblastic dike formation. The ilmenite solid solutions in the granoblastic dikes are also different from the primary, near-pure ilmenite of the lava pond in their high hematite contents [*Dziony et al*., 2008].

The present study involves an analysis of 316 samples collected from core pieces throughout the entire hole. One hundred seventeen samples cover the interval of Leg 206, 152 of Leg 309, and 47 of Leg 312. The extrusive rock pile comprises 186 samples, the sheeted dike complex 100, and the gabbro 30. Samples were primarily collected for remanent magnetization and paleointensity determinations and accompanying rock magnetic property analysis [*Herrero-Bervera and Acton*, 2011; *Herrero-Bervera et al*., 2011; *Krása et al*., 2011].

3. Magnetic Parameters and Methods

We base our interpretation on magnetic parameters, specifically the coercive force (B_c), the coercivity ratio (B_{cr}/B_c, where B_{cr} stands for remanent coercivity), magnetization ratio (the ratio of the saturation magnetization (M_s) and remanent saturation magnetization (M_{rs})), low-field magnetic susceptibility (χ_{in}), and the Curie temperature (T_C). Their downhole trends are discussed in *Herrero-Bervera et al*. [2011] and here we focus on their multivariate statistical interpretation. Measurements were performed at the magnetic laboratories of the University of Hawaii (Honolulu, USA) and the University of California, Davis (USA). An alternating gradient force magnetometer (MicroMag, Model 2900) with a maximum field of 1.2 Tesla in the Davis laboratory was used for room temperature hysteresis loop measurement. Typical signals (sample mass 4–10 mg) were at least four orders of magnitude above the noise level of the instrument ($\sim 2 \times 10^{-10}$ Am^2). In the Honolulu laboratory a variable force translation balance (VFTB, Petersen instruments, sample mass ~200 mg) was utilized with a maximum field of 1 Tesla. Both sets of hysteresis loops were corrected for paramagnetic contribution by subtracting the high field slope (calculated from magnetizations in fields higher than 0.7 Tesla); B_c was obtained from the slope-corrected loop by linear interpolation between the field steps where the magnetization changed sign. For determination of the Curie temperature, samples were heated to 700°C in a field of ~720 mT in the VFTB instrument. Sample magnetizations were at least two orders of magnitude above instrumental noise level ($\sim 1 \times 10^{-8}$ Am^2). In cases of multiple Curie temperatures, the dominant temperature (usually the lowest) is taken to be characteristic of the sample. Low-field susceptibility data

were acquired at room temperature with an AGICO (Brno, Czech Republic) KLF sensor or with a KLY2 susceptometer; the susceptibilities were several orders of magnitude stronger than instrumental noise levels (5×10^{-6} SI and 4×10^{-8} SI, respectively, for a nominal sample volume of 10 cm^3).

4. Multivariate Statistical Techniques

Simultaneous evaluation of effects of multiple input parameters is possible with multivariate statistical techniques. A myriad of options exist, each with specifics tailored to a type of data, a particular problem at hand, etc. [e.g., *Höppner et al*., 1999]. Here, we use fuzzy c-means clustering (FCM) and nonlinear mapping (NLM). Examples in geosciences related to rock magnetics include the analysis of early diagenetic effects on the Calabrian Ridge sediments collected with a long piston core [*Dekkers et al*., 1994], variations in the expression of surface sediments in the Southern Atlantic Ocean [*Schmidt et al*., 1999], the unraveling of the impact of anthropogenic effects on a soil-data set from Austria [*Hanesch et al*., 2001], and an analysis of climate change from piston core data in the Azores area [*Vlag et al*., 2004]. A recent sedimentological example is the study by *Lucieer and Lucieer* [2009] on ocean sediments off the shore of Australia with gradual spatial boundaries that are classified in terms of provenance with the help of FCM and NLM.

The following summarizes the strategy and principles adopted for the interpretation of the present data set. Cluster analysis, whatever its exact formulation, should be performed with reasonably symmetrically distributed input parameters. The basic physical interpretation of each parameter must also be understood to provide a firm basis for the multivariate interpretation. For the present study, the basic meaning of the five magnetic input parameters is: χ_{in} is a measure of the concentration of the Fe-Ti oxides and T_C is a measure of the dominant composition of those Fe-Ti oxides. B_c, B_{cr}/B_c, and M_{rs}/M_s were chosen as grain-size indicators. Thus, a parameter set is selected that in essence reflects the behavior of the Fe-Ti oxides in terms of concentration and composition and with emphasis on subtle grain-size effects. Information on incipient oxyexsolution is also reflected by changes in Curie temperature. Other potential hydrothermal effects may also be identified by changes in grain-size. We use classic hysteresis parameters, supplemented with χ_{in} and T_C, primarily because these measurements are available for the entire sample set; however, we are aware that they cannot describe the variability within the data to the full. Future studies may consider further parameters to provide a more detailed picture of certain aspects of the data set. Later, in section 6.1, we will suggest some prospective parameters that can be acquired at room temperature.

A multivariate data cloud is rarely homogeneous and processes that have acted on the samples may lead to grouping in the data. Groups or clusters within a multidimensional data cloud convey meaning as to why they exist and how groups can evolve with respect to each other. If such meaningful groups can be extracted from a certain data set, the researcher has a powerful interpretational tool at hand. However, groups within a data set are seldom known in advance and so-called unsupervised partitioning techniques, such as clustering, are required for their identification. Clustering techniques partition samples or "cases" over a user-specified number of subgroups (i.e., clusters) based on a similarity measure. Classic hard clustering techniques allocate each case to one cluster only which may lead to distorted clusters if the samples are not that alike. Importantly, gradual changes are difficult to portray with hard clustering. Fuzzy clustering techniques, of which FCM is one, calculate the similarity of a case to all clusters considered. This similarity is expressed by a membership for each cluster that varies between 0 (no similarity) and 1 (completely identical). For every case, the memberships to all clusters considered sum to 1. In FCM, the cases are iteratively partitioned over the desired number of clusters in such a way that the cases are as close as possible to their cluster center while simultaneously the cluster centers are as far away from each other as possible. Samples that cannot be allocated to a specific cluster have appreciable memberships to more than one cluster. As such gradual boundaries can be visualized. In order to have equal weight for each input variable, data were standardized (i.e., each variable was normalized to have a mean of 0 and a standard deviation of 1).

Selecting the optimal number of clusters, the cluster validity, is an essential part of the entire clustering procedure, since the number of groups is not known a priori [*Dave*, 1996; *Wu and Yang*, 2005]. Over the years FCM users have proposed a set of validity functionals or validity indices that mathematically judge the cluster solution. Classic functionals, the partition coefficient (PC), and partition entropy (PE) [*Bezdek*, 1974; *Bezdek et al*., 1984; *Bezdek*, 1992], only define compactness, with the optimal number of

clusters being defined by the maximum PC and by the minimum PE. *Dave* [1996] has proposed a modified partition coefficient (MPC, maximal for an optimal number of clusters) to reduce the tendency of the PC toward low cluster numbers. More recent validity indices measure the degree of compactness and separation between all clusters. They include the XB index (minimal; *Xie and Beni* [1991]), the PMBF index (minimal; *Pakhira et al*. [2005]), and the PCAES index (maximal; *Wu and Yang* [2005]). Logically, an optimal cluster should be compact and clearly separated from the others. In practice, gradual boundaries make the isolation of "crisp" clusters often impossible. Cluster validity indices try to capture the robustness of the cluster solution in a single numerical value. Often the various indices do not infer the same number of clusters to be optimal [e.g., *Lucieer and Lucieer*, 2009]. Thus indices should not be treated as definitive model selection criteria, but instead as indicative parameters. To contribute to this issue, we take a probabilistic approach with the help of the distance metric of *Torres et al*. [2008]. The FCM iteration procedure is known to be sensitive to the starting configuration used to initiate the algorithm. We consider a solution robust when the samples are always allocated to the same cluster independent of the starting configuration. Therefore, for each number of clusters (two through nine clusters), the models were run from 500 starting configurations spanning the entire data space. Each solution was pair-wise compared with the distance metric of *Torres et al*. [2008] which yields 0 if two cluster solutions are identical and 1 if they are completely inconsistent. Thus, when the distance metric starts to deviate from 0 for a given number of clusters, the solutions are displaying a dependence on starting configuration and must be deemed unreliable. The highest number of clusters which yielded only distance metrics of 0 is thus considered to be the optimal model.

The cluster solutions were further assessed by low-dimensional graphical representations. Nonlinear mapping [*Sammon*, 1969] has been shown to be a very useful tool to this end [e.g., *Vriend et al*., 1988]. With an increasing number of clusters, the allocation from the FCM algorithm and the nonlinear mapping projection must remain coherent; otherwise "interpretational noise" is the result. *Abonyi and Babuska* [2004] proposed to map the samples and the cluster centers onto the projection plane with a modified algorithm that also maintains distances between the clusters and the data points. Their two-dimensional NLM projection plane (termed Sammon projection) aims to preserve the distances between the data within the original data set (in this case a five-dimensional data cloud). They calculate membership contours that are also plotted. With their FUZZSAM algorithm, they project the results of FCM onto the projection plane whereby the normal Sammon projection serves as initialization, the samples' cluster memberships are also taken into account. The so-called FUZZSAM projection conveys the fine structure within clusters better than the normal Sammon projection. Transitional samples (with no dominant membership) should fall in areas in the plot where the hyperspheric membership contours of several clusters meet [*Abonyi and Babuska*, 2004]. Further, in a robust solution the number of transitional cases (samples with the second highest membership ≥ 0.6 times the dominant membership) should not be that large.

Another way to handle transitional cases is to plot the so-called confusion index (CI) [*Burrough et al*., 1997, 2000]: when the memberships of two or more clusters become (nearly) equal, there is uncertainty concerning the cluster allocation, conversely if one membership dominates there is little doubt on the cluster allocation. Broad transition zones convey gradual trends within the data while small transition zones indicate crisp boundaries. In this way, dominant and more subtle processes may be elucidated. The CI pattern is mapped here on the Sammon and FuzzSam projections of *Abonyi and Babuska* [2004]. The CI and Sammon plots are used along with cluster validity indices to decide upon the optimal number of clusters: coherent "cluster regions" should appear, otherwise there is a risk of overinterpreting the data structure. As mentioned earlier, validity indices are adopted as model selection guidelines. Indices that evaluate compactness only appear to describe first-order properties of the data sets. Those that take separation into account to some extent describe finer features as well.

The various map visualizations are particularly useful tools to gauge the robustness of the solutions with an increasing number of clusters. Solutions were calculated iteratively (until the difference in the objective function between consecutive iterations became $< 10^{-4}$) from two up to nine clusters, i.e., a number where the cluster allocations became clearly blurred at a point exceeding the algorithm's discriminative power. The stability of cluster solutions generated from different starting positions was given considerable interpretational weight along with coherency in the CI and Sammon plots.

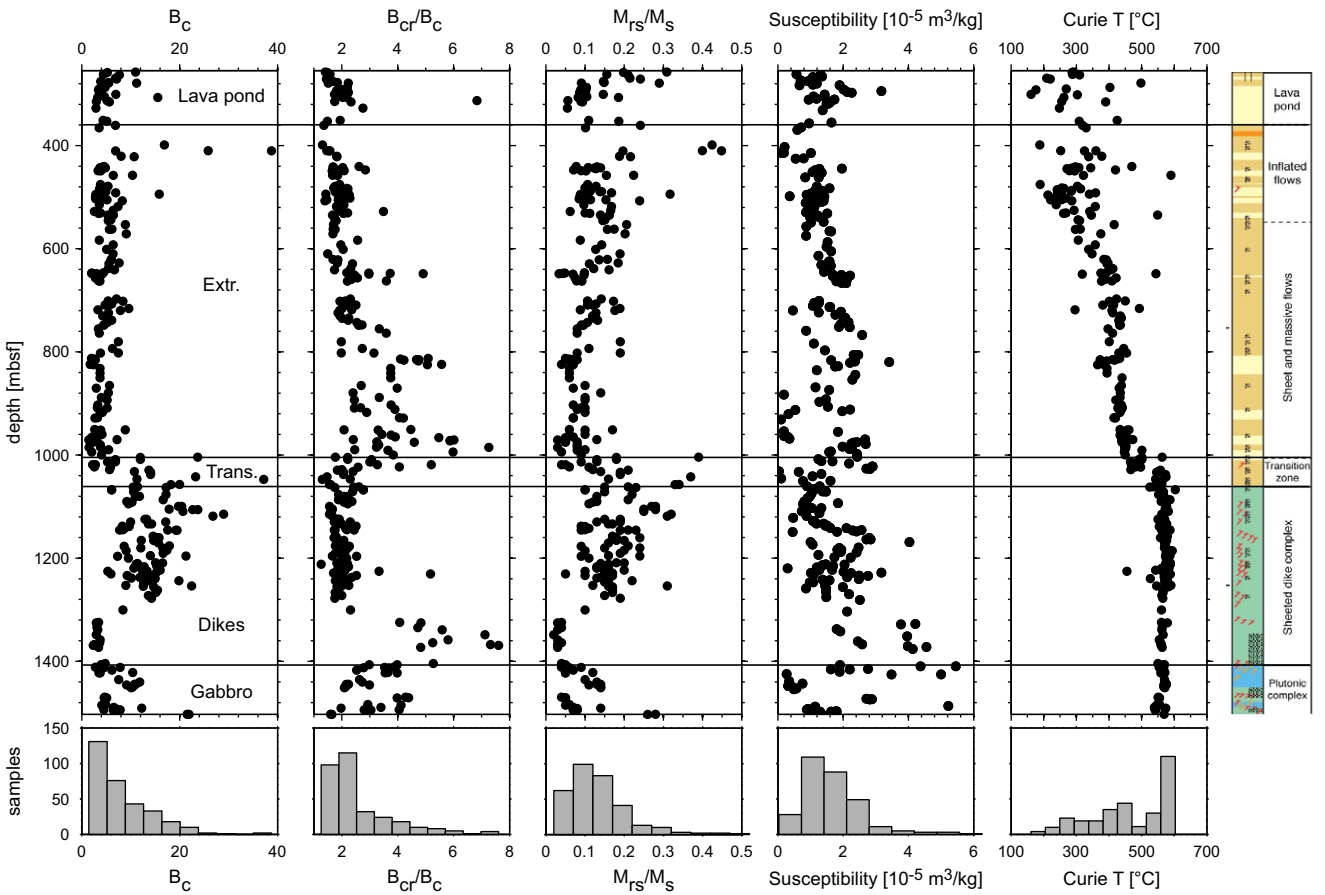

Figure 1. Downhole plots (adapted from *Herrero-Bervera et al.* [2011] and *Teagle et al.* [2006]) and histograms of input variables. B_c = coercive force (mT), B_{cr}/B_c = coercivity ratio, M_{rs}/M_s = magnetization ratio, Curie T = Curie temperature (°C). "Lava pond" = off-axis very thick lava flows, Extr. = extrusive section, Trans. = transition zone between extrusives and sheeted dikes, Dikes = sheeted dike complex, Gabbro = isotropic gabbro part. Lithology column: light yellow = massive basalt, beige = sheet flow, light brown = pillow basalt, green = sheeted dike, blue = gabbro. Intrusive contacts are indicated with red symbols and magmatic contacts with beige symbols. Breccia is indicated with black symbols in the middle of the lithological column while granoblastic texture is indicated with finer black symbols at the right side of the lithological column.

5. Results

5.1. Input Parameters

The patterns and trends described below are dealt with in considerably more detail in *Herrero-Bervera et al.* [2011] along with scanning electron microscope (SEM) pictures demonstrating (incipient) exsolution in *Krása et al.* [2011]. Downhole trends of the input parameters are plotted in Figure 1 (adapted from *Herrero-Bervera et al.* [2011]). Coercive force ranges between ~2 and ~10 mT in the extrusive rocks with occasionally higher values in the inflated flow section. There is an overall tendency for B_c to decrease with increasing depth to the dike transitional zone. The upper dike section shows a variable B_c behavior with higher values ranging between ~10 and ~20 mT, whereas the lower (granoblastic dike) section is characterized by low B_c values of ~3–4 mT. The gabbros have higher B_c values of ~5–10 mT. The dike screen between the gabbro layers has notably low B_c values while B_c of the deepest basaltic dikes is comparable to that of the sheeted dikes. The magnetization ratio (M_{rs}/M_s) is variable as well (range ~0.05 – ~0.25 with occasional values up to 0.4); it tends to decrease with increasing depth within the lavas. The sheeted dikes have values similar to the upper half of the lavas. The granoblastic overprinted section, however, has the lowest M_{rs}/M_s values of the entire core of ~0.02 – ~0.04. In the gabbroic parts, M_{rs}/M_s rises again but does not reach typical sheeted dike values. The coercivity ratio (B_{cr}/B_c) is distinctly less variable; most of the lavas and sheeted dikes have B_{cr}/B_c of ~2. Within the extrusive rock pile B_{cr}/B_c tends to increase with depth from ~700 mbsf downward. The granoblastic dikes have notably high coercivity ratios. B_{cr}/B_c varies between ~2 and ~4 in the gabbro. χ_{in} varies more deeply down in the core. Within the extrusive rocks, an overall increase with depth is notable. The sheeted dikes are typified by low values in their top part comparable to values

Table 1. Validity Indices as a Function of Number of Clusters[a]

Validity Indices	Standardized Input Data							
Cluster	Max PC	Max MPC	Min PE	Min PEsc	Min XB	Min PBMF	Max PCAES	Min DM
2	***0.668***	0.336	***0.503***	0.473	3.112	3.277	1.959	0.0000
3	0.614	***0.422***	0.687	***0.423***	2.649	3.164	***2.359***	0.0055
4	0.528	0.371	0.897	0.465	**1.826**	3.059	2.047	0.0000
5	0.480	0.350	1.041	0.479	2.027	3.003	1.572	***0.0000***
6	0.442	0.330	1.170	0.496	2.070	2.952	0.952	0.0440
7	0.420	0.324	1.265	0.502	**1.640**	2.896	0.874	0.2199
8	0.406	0.321	1.344	0.505	1.701	2.841	0.460	0.0477
9	0.387	0.311	1.426	0.513	***1.530***	***2.810***	0.653	0.2531

[a]PC = partition coefficient (maximal), MPC = modified partition coefficient [*Dave*, 1996] (maximal), PE = partition entropy (minimal), PEsc = scaled partition entropy (minimal, the actual value is rescaled as a fraction between 0 and 1 to the distance between the minimum and maximum value for each number of clusters), XB = Xie-Beni index [*Xie and Beni*, 1991] (minimal), PBMF = Pakhira-Bandyopadhyay-Maulik Functional [*Pakhira et al*., 2005] (minimal), PCAES = partition coefficient and exponential separation index [*Wu and Yang*, 2005] (maximal). DM = average distance across ensemble of pair-wise compared cluster solutions [*Torres et al*., 2008]. Optimal validity measures are indicated by numbers in bold italics, other favorable cluster solutions in bold.

obtained for the lava pond. With depth, χ_{in} tends to increase again with the highest values for the granoblastic dikes. The gabbros have notably low χ_{in} values with the intervening dike screen values comparable to the granoblastic dike part. The Curie temperature in the extrusive rock section varies between ~250 and ~450°C with an overall tendency to increase with depth. A spinodal exsolution model to explain the increase of the Curie temperature with depth throughout the extrusive section of the core is provided in *Krása et al*. [2011]. Occasionally high T_C values of up to ~580°C occur, possibly related to later intruded dikes. The T_C of the topmost 350 m of the lavas is more variable than below. In the dike transition zone, T_C rapidly increases to ~580°C; this T_C, indicative of magnetite devoid of Ti, remains constant throughout the dikes and gabbros.

5.2. Interpretation of the Optimal Cluster Model

Histograms of the five input variables are shown in Figure 1. Before running the FCM algorithm, the input parameters were standardized and scaled to give each input variable equal weight. Validity indices as a function of the numbers of clusters (Table 1) do not clearly point to a specific cluster solution that would be mathematically preferable over others. The classic indices (PC and PE, known to be conservative concerning the optimal number of clusters) favor two clusters, reasonably consistent with a division according to extrusive lavas on the one hand and sheeted dikes and gabbros on the other. The MPC and the scaled PE (PEsc) indicate three clusters. However, throughout the extrusive sequence, several levels with "intrusive" signatures are obtained, and virtually none of those samples has a high T_C that could point to later sill or dike intrusion. Also notable is that some gabbro and dike samples have characteristics similar to extrusives. In particular, the gabbro section of the hole appears to have distinctly varying magnetic properties. Evidently, multiple intrusion, hydrothermal, early, and late metamorphic effects complicate a simple separation. Further inspection of the Sammon and FuzzSam maps indicate that more structure is visible, so a number of clusters >2 is appropriate. Therefore, solutions with an increasing number of clusters are considered. Validity indices that also take cluster separation into account—XB, PBMF, and PCAES—indicate as optimal cluster number 9 (with local minima at four and seven clusters), 9 (actually the index "optimizes" from two clusters onward), and 3, respectively. However, from eight clusters upward, samples with a clear cluster affiliation appear to plot in the field of other clusters in an increasing number of occasions on the Sammon and FuzzSam maps. This indicates there is a large risk that "data noise" is being interpreted and solutions for cluster numbers ≥8 were not considered further. Five, six, and to a lesser degree, seven cluster solutions appear to be visually consistent on the Sammon and FuzzSam maps and are supported by reasonably high values of the PCAES index that is often regarded as the preferred cluster validity index (particularly the five cluster solution has fairly high values). Importantly, the cluster solution starts to become dependent on the starting configuration of the data from six clusters and higher as expressed by the distance metric DM (Table 1). Therefore, we consider a five cluster model optimal; the cluster centers are given in Table 2 and Sammon and FuzzSam maps are shown in Figure 2.

Logically, the cluster model should be interpreted according to general magmatic and alteration principles and their bearing on magnetic properties. The dominant titanomagnetite in mid-ocean ridge basalts is

Table 2. Cluster Centers of the Five Cluster Solution[a]

Standardized	ExPr	ExA	ExM	InP1	InP2
B_c (mT)	5.186	4.980	3.303	11.277	18.264
M_{rs}/M_s	0.130	0.091	0.047	0.143	0.230
B_{cr}/B_c	1.886	2.795	4.722	2.142	1.750
χ_{in} (m^3/kg)	1.26	1.75	2.65	1.38	1.26
T_C (°C)	305	443	495	551	558

[a]Cluster centers are ranked according to increasing Curie temperature. B_c = coercive force (mT), M_{rs}/M_s = magnetization ratio, B_{cr}/B_c = coercivity ratio, χ_{in} = low-field susceptibility (in units of 10^{-5} m^3/kg), T_C = Curie temperature (°C). ExPr = extrusive pristine, ExA = extrusive altered, ExM = extrusive altered multidomain, InP1 = intrusive pseudo-single-domain 1 and InP2 = intrusive pseudo-single-domain 2. For interpretation, see main text.

variably maghemitized ($Fe_{2.4}Ti_{0.6}O_4$ or TM60 with a Curie temperature range of ~160–380°C (e.g., *Lattard et al*., [2006]; Fe_3O_4 is TM0 and Fe_2TiO_4 is TM100). In Hole 1256D, the grains are partially maghemitized at a level that remains more or less constant downhole down to the lowermost portion of the sheeted dike complex ($z \sim 0.6$; *Krása et al*. [2011]). Note that the analysis of *Krása et al*. [2011] was restricted to larger magnetic particles (> 10 μm) that contain the entire spot of the SEM energy dispersive spectrometer set-up so that the analyses are not contaminated by neighboring particles. We distinguish three clusters with an extrusive rock signature—Extrusive Pristine (ExPr), Extrusive Altered (ExA), and Extrusive Multidomain (ExM)—and two clusters with intrusive features—Intrusive Pseudo-single-domain type 1 and 2, respectively (InP1 and InP2). Coercive force and Curie temperature appear to be the foremost discriminators. With increasing hydrothermal alteration, T_C goes up in the extrusive section while all sheeted dike and gabbro samples have T_Cs around 580°C, indicative of pure Fe_3O_4. The latter often have notably high B_c values with related high M_{rs}/M_s.

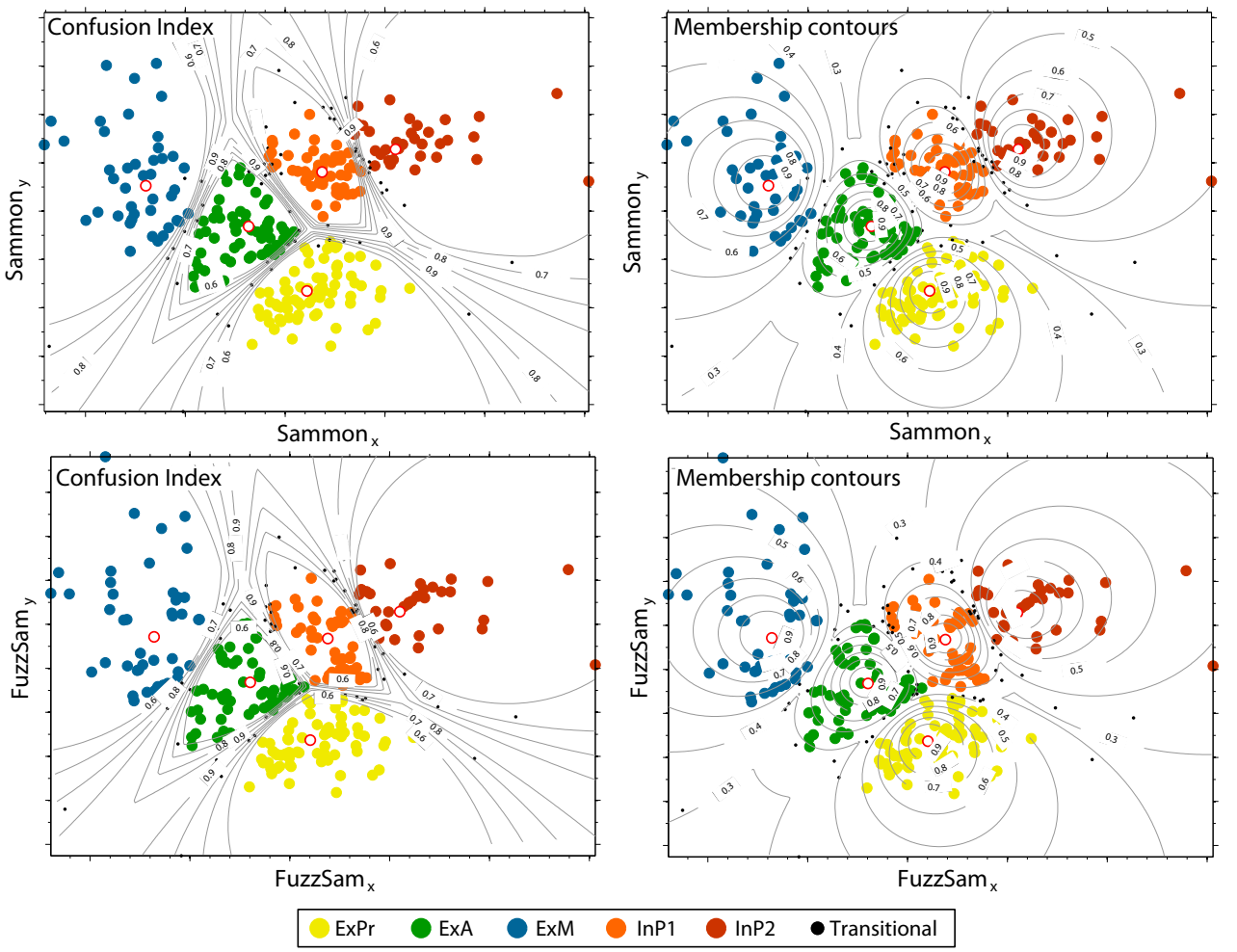

Figure 2. Sammon and FuzzSam maps for the five cluster solution. Hyperspherical maximum membership contours are according to *Abonyi and Babuska* [2004]. The confusion index is from *Burrough et al*. [1997]. Transitional samples, where the second highest membership takes a value of more than 60% of the highest membership, are marked as small black points.

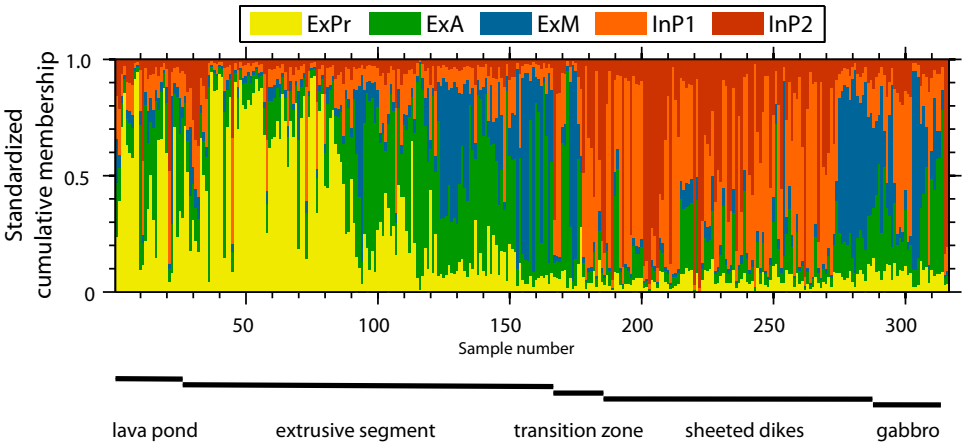

Figure 3. Membership distributions for all samples plotted versus sample number. The corresponding lithological segment (cf. Figure 1) is indicated below. ExPr cluster: light green, ExA cluster: dark green, ExM cluster: dark blue, InP1 cluster: dark brown, and InP2 cluster: light brown. ExPr cluster samples appear to be dominant in the top part of the extrusive zone followed downward by ExA and then ExM. In the deepest extrusive parts, ExA and ExM samples occur, both testifying to the scattered nature of the alteration.

The ExPr cluster center has the lowest T_C and is interpreted as representing (approximately) pristine ocean crust. B_c, M_{rs}/M_s, and B_{cr}/B_c indicate rather coarse PSD grains. χ_{in} of this cluster is comparatively low. Samples with high T_C and high B_c and M_{rs}/M_s (seen on the periphery of this cluster, Figure 2) are interpreted as grain fining by incipient oxyexsolution as supported by SEM observations [*Krása et al*., 2011].

With increasing alteration, the magnetic particles oxyexsolve and the cluster ExPr grades to ExA and then to ExM. As alteration progresses Curie temperatures increase further and (titano)magnetite (in a broad sense, including variably maghemitized compositions) lamellae become larger resulting in hysteresis ratios moving progressively toward and into the MD field. Note that χ_{in} increases as anticipated by the generation of more increasingly Ti-poorer magnetite of which intergrowth features become larger as well. The intrusive clusters InP1 and InP2 are characterized by Curie temperatures of ~550–570°C indicative of (almost) pure magnetite. Yet, their hysteresis ratios are PSD and fine PSD, respectively, and χ_{in} is low, comparable to that of the ExPr cluster. Because of prolonged higher temperatures, intermediate titanomagnetite has exsolved to particles consisting of magnetite and ilmenite lamellae, with a magnetic grain size much finer than the physical grain size. Indeed SEM photographs show magnetite with ilmenite lamellae and ilmenite with finely exsolved magnetite [*Krása et al*., 2011].

6. Discussion

6.1. Comparison of the Clustering of Magnetic Parameters with Lithology

Figures 3 and 5 show the downhole distribution of sample membership to each cluster. As anticipated, the most pristine samples are confined to the top segment of the hole: below ~641 mbsf only a few scattered "pristine" samples occur. Noteworthy is that the lower portion of the lava pond contains a fair number of samples allocated to the ExA cluster. So, even the topmost section, lava pond is not devoid of alteration phenomena. From ~630 mbsf to ~1023 mbsf (well within the transition zone to the sheeted dikes), ExA and ExM clusters are prominent. More altered ExM samples have a slight tendency to occur in the deeper portion. The cluster analysis allows an assessment on a "per sample" basis, enabling a refined picture of the overall downward progression in alteration. The transition zone between the extrusive sequence and the sheeted dikes behaves magnetically as intrusive. Throughout the extrusive sequence, a few scattered samples occur that are classed as intrusive, 10 in total (out of 166 samples). For the two topmost of these deviating samples (in the lava pond at 278.91 and 306.81 mbsf), the Curie temperature was not measured (in such cases, the algorithm replaces missing values with the cluster center value at each iteration in order to not distort the calculation) and since their hysteresis properties are "intrusive-like" they are classed as such in InP2. Adjacent samples have low Curie temperatures. It may well be that the deviating samples represent the very first, comparatively dry, stage of exsolution leading to grain fining. For three other samples (409.89, 410.07, and 494.28 mbsf) with measured low Curie temperatures, the same reasoning applies. The impact

of SD-like hysteresis properties outweighs that of the low Curie temperature in the FCM and samples are classed as InP2. They could well represent an initial "dry exsolution" stage.

The other five samples (457.65, 534.64, 715.95, 802.15, and 951.15 mbsf with Curie temperatures of 590, 549, 493, 430, and 461°C, respectively) are classed to the InP1 cluster despite three cases having fairly low Curie temperature for the InP1 cluster. Apparently the influence of the hysteresis parameters outweighs that of the Curie temperature in the FCM analysis. According to the log descriptions of the volcanostratigraphy, only the sample at 951.15 cm comes from a dike. The two highest samples (at 457.65 and 534.62 mbsf) have a high Curie temperature and behave magnetically like intrusives despite their classification as being from basaltic sheet flows. Possibly the core of the sheet flow had sufficient time to create exsolved titanomagnetite. It should be realized that the limited number of input parameters cannot describe all natural variability, resulting in a few somewhat counterintuitive samples in the clusters.

Magnetic clusters with intrusive features, InP1 and InP2, are dominant from ~1030 mbsf down to ~1230 mbsf (Figure 5), starting ~30 m higher uphole than where sheeted dikes are described in the logs. In the transition zone, a number of intervals have dike lithologies based on core descriptions [*Teagle et al*., 2006]. The topmost portion of the transition zone with dikes described in the log is so altered that its samples are classified as being in altered clusters. Below this altered zone, as expected, an intrusive signature emerges from the magnetic properties from all samples. Below 1230 mbsf, the intrusives are allocated to the ExM cluster and not to either intrusive cluster. They have a high T_C but are notably multidomain. Since the grain-size information gets more weight than the Curie temperature in the calculation of the cluster model (three variables versus one), this has led to their allocation to ExM, a cluster that expresses extrusive rock properties. This indicates that one should never blindly rely on cluster allocations without inspection of the down-hole trends in clusters. The granoblastic overprint in the lowermost dikes [*Koepke et al*., 2008; *Krása et al*., 2011] has generated an entirely new magnetite population that lacks the intergrown lamellae resulting in MD particles. This highlights the idea that one should always consider the cluster affiliation of samples in conjunction with the individual input parameters. Identifying granoblastically overprinted samples in a separate cluster (as would be conceivable) is apparently beyond the power of the present set of input variables.

The gabbro zone (deeper than 1406 mbsf) appears to be remarkably complex from a magnetic mineral point of view. Magnetic grains are often coarser than in the dikes leading to classification in altered extrusive clusters in a substantial number of samples. This could be a consequence of multiple gabbroic intrusions. Also the dike screens are granoblastically overprinted leading to allocation to ExA or ExM clusters. For a better distinction of the gabbros, other magnetic parameters expressing grain size and alteration, for example related to the anhysteretic remanent magnetization, could be included in the analysis. Alternatively, a parameter that accounts for the greater variability in all rock magnetic parameters might be able to differentiate the complex gabbro zone from the less variable ExA and ExM clusters.

The hysteresis parameters are plotted on a "Day plot" [*Day et al*., 1977] for the five cluster solution and the defuzzified version (Figures 4a and 4b; defuzzified means that the highest membership is used to make a hard cluster assignment of each sample, so no transitional samples can occur; this is equivalent to conventional hierarchical c-means clustering). Note that the samples plot close to the SD-MD mixing line of *Dunlop* [2002], indicating the contribution of SP particles is insignificant. Only for the highest B_{cr}/B_c values, the samples plot slightly above the SD-MD mixing line. Both defuzzified plots have a rather scattered appearance particularly with a rather large overlap between the ExPr and InP1 clusters. When considering the memberships many samples from the overlaps appear to be transitional, with appreciable memberships to more than one cluster. This clearly illustrates the merit of the fuzzy approach which enables visualization of ambiguities. It also shows that a two-dimensional representation of the five-dimensional data space is an oversimplification of reality, although the cluster allocation is coherent in terms of the hysteresis parameters. The ExPr cluster plots below the InP1 and InP2 clusters, so extrusive rocks (when not altered too much) have hysteresis properties distinct from dikes and gabbros (again when not altered too much). However, cluster fields partially overlap on the Day plot, which makes a firm distinction based solely on hysteresis properties ambiguous. Alteration trends of the extrusive samples on the Day plot are subtle. The most pristine samples in the ExPr cluster plot around M_{rs}/M_s ~0.1 and B_{cr}/B_c ~2. Samples that show incipient alteration move toward the SD field (M_{rs}/M_s ~0.15 and B_{cr}/B_c ~1.8). Further alteration reverses this trend and with progressing alteration samples move back toward (ExA cluster) and into the MD field (ExM cluster).

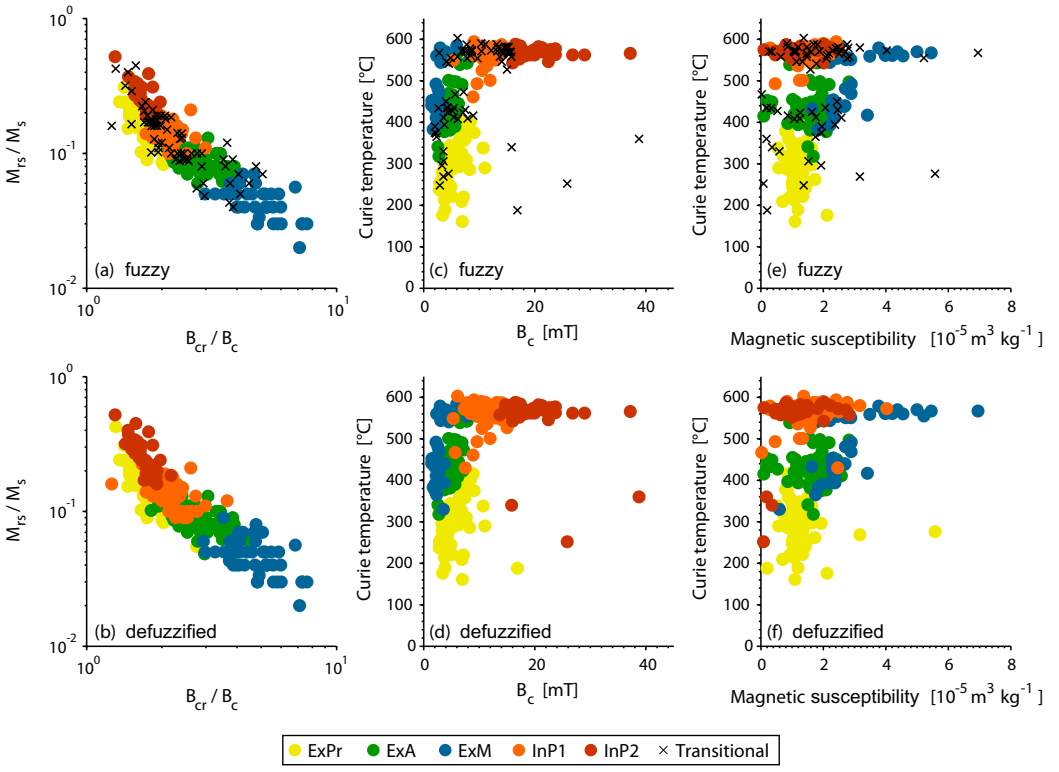

Figure 4. Trends in hysteresis parameters as a function of alteration plotted on a Day plot, coercive force versus Curie temperature, and susceptibility versus Curie temperature; fuzzy (with transitional samples, indicated by crosses) and defuzzified (without transitional samples) plots are shown. (a and b) Day plot: The most "pristine" lava samples (ExPr, light green) first grade to ExA (dark green) with increasing alteration and then to ExM (dark blue). Dikes and gabbros (clusters InP1 and InP2, light and dark brown, respectively) plot on a distinct trend overlapping but slightly above the trend of the ExPr cluster. In substantially altered samples, the intrusive and extrusive trends overlap on the Day plot, alteration masks their provenance. (c and d) Coercive force versus Curie temperature: ExPr samples have lowest Curie temperature while that of ExA and ExM overlaps. ExM has lowest coercive force. InP1 and InP2 samples are discriminated primarily based on their coercive force. (e and f) Susceptibility versus Curie temperature: ExPr and ExA have similar susceptibility while ExM has highest susceptibility, both for Curie temperatures up to 500°C (extrusive segment) and around 550–570°C (intrusive segment). InP1 and InP2 have similar susceptibility. "Fuzzy" plots appear to be distinctly more coherent than the equivalent defuzzified plots, indicating that many of the "deviating" samples are classed to be transitional. This clearly hints at the gradual character of the processes involved that can be conveniently described with the fuzzy approach.

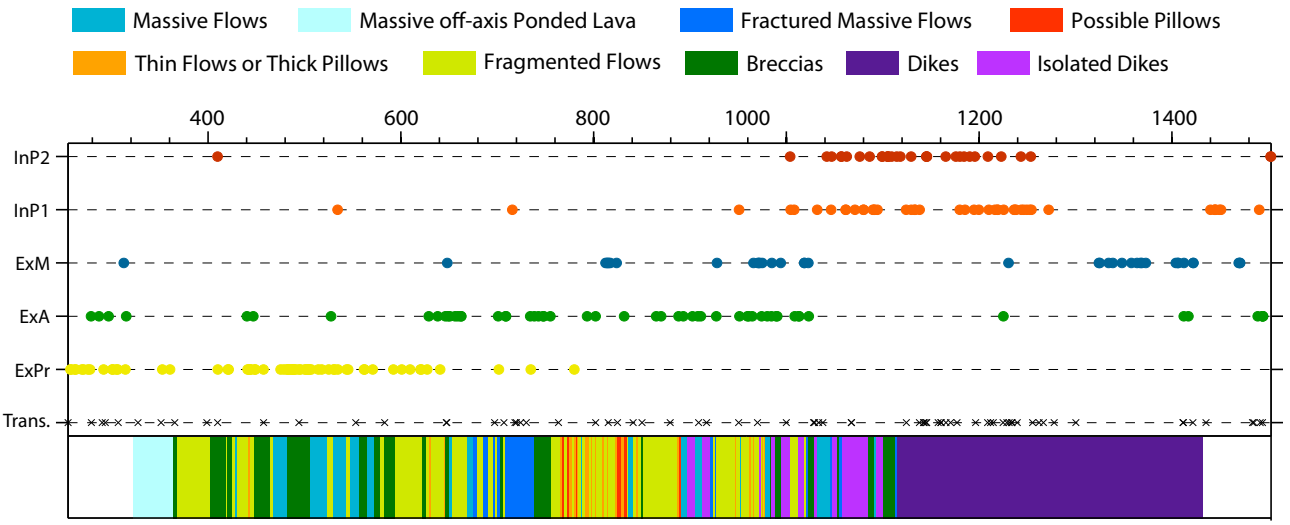

Figure 5. Downhole cluster affiliation of the samples for the five cluster solution (marked as FCM). "Trans." (transitional) indicates that the second highest membership takes a value of more than 60% of the highest membership. The simplified lithology is the artificial neural network classification of *Tominaga et al.* [2009] based on several logging tools applicable to the extrusive and sheeted dike intervals of the hole while the cluster results come from cored material of the entire hole.

Also the division between extrusives on the one hand and dikes and gabbros on the other has disappeared. Thus, it is not possible to make a firm distinction based on hysteresis properties alone. The secondary magnetite formed during metamorphic processes has no intergrowths [*Krása et al*., 2011]. When discriminating between these samples, the Curie temperature is an important diagnostic parameter. Samples with $T_C > 520°C$ (~50% of the cases) are nearly always associated with dikes and gabbros. A few levels are assigned to clusters with intrusive features based on their hysteresis properties, apparently outweighing the influence of a comparatively low T_C. This strongly indicates that these particular levels have undergone alteration.

To further illustrate how the cluster distribution is visualized on scatterplots, we show also plots of B_c versus T_C and χ_{in} versus T_C (Figures 4c–4f). The extrusive sequence shows a fairly broad B_c range for lowest T_C, i.e., the most pristine cluster ExPr (Figures 4c and 4d). The ExA and ExM clusters have similar T_C with ExM having lowest B_c. There appears to be a fair number of transitional cases throughout the field of the ExA cluster. In the T_C range of ~550–580°C, the InP1 and InP2 clusters are typified by $B_c > \sim 10$ mT. The cluster containing samples with the lowest B_c values is ExM, with a few cases of ExA. All of these samples come from the sheeted dikes and gabbro. The alteration manifested by low B_c likely is either representing granoblastic dikes with MD particles of pure magnetite due to granulite facies metamorphism, or altered portions with bigger lamellae that magnetically interact leading to low B_c values. Transitional cases are restricted to B_c values $< \sim 17$ mT. Note that the four deviating samples with notably high B_c and low T_C are all transitional, showing the merit of the fuzzy approach.

The cluster fields also emerge coherently in the plots of χ_{in} versus T_C (Figures 4e and 4f). The intrusive clusters InP1 and InP2 plot on top of one another, thus susceptibility cannot discriminate between those clusters. The ExM cluster is characterized by highest χ_{in} values and $T_C > \sim 380°C$. ExA plots roughly above ExPr with ExM at its highest χ_{in} portion. Interestingly, nearly all deviating samples appear to be transitional, again demonstrating the suitability of a fuzzy approach.

The present interpretation is based on five routine mineral magnetic parameters. For a more refined interpretation, additional parameters would be advantageous. These could include measurement of the frequency dependence the low-field susceptibility to quantify any superparamagnetic (SP) particles. Further, the intensity of the anhysteretic remanent magnetization (ARM) and the susceptibility of the ARM (the ARM intensity divided by the direct bias field used to induce it) to represent SD and fine PSD behavior in a manner complementary to hysteresis properties. Where appropriate, parameters should be expressed on a mass-specific basis to enable proper comparison. Other parameters would include S-ratios retrieved from acquisition curves of the isothermal remanent magnetization and back field demagnetization curves. The classic interpretation of the S-ratio in terms of magnetite and hematite should be treated with some caution in such data sets, because titanomagnetite can have a high coercivity tail beyond 300 mT which would be erroneously attributed to hematite. Also, more sophisticated parameters to describe the shape of the hysteresis loop could be considered. *Fabian* [2003] proposed a shape parameter: $\sigma_{hys} = \ln(E_{hys}/4*B_c*M_s)$, where E_{hys} is the area contained by the branches of the hysteresis loop. E_{hys} is $> 4*B_c*M_s$ for so-called wasp-waisted loops while potbellied loops are characterized by $E_{hys} < 4*B_c*M_s$ [*Fabian*, 2003]. Another parameter proposed by *Fabian* [2003] is the ratio of the transient energy dissipation to E_{hys}. This requires the additional measurement of a first-order-reversal curve starting at zero field, which can be easily implemented in a hysteresis loop measurement scheme. Plotting this ratio against σ_{hys} would enable discrimination of SP and MD particles which is not so straightforward from more classic rock magnetic parameters.

6.2. Comparison of the Clustering of Magnetic Parameters with a Log-Based Electrofacies Analysis

Tominaga et al. [2009] have developed a volcanostratigraphic framework for Hole 1256D based on electrofacies, which is derived from images collected by Formation Microscanner (FMS) and Ultrasonic Borehole Imager (UBI) logging tools (Figure 5). They adopted an artificial neural network approach to distinguish grouping in their data. The electrofacies-based division discriminates primarily on the basis of porosity which is tied to (hydrothermal) alteration. The lava pond and gabbro portions of Hole 1256D were not considered by *Tominaga et al*. [2009] because they are not sufficiently porous to yield meaningful, interpretable, logs. Below the lava pond, intervals of massive and fractured massive flows alternate with fragmented flows and breccias down to a level between 700 and 780 mbsf, where many more thin flows or thick pillows and possible pillows are distinguished. Further down isolated dikes occur increasingly often with increasing

depth. *Tominaga and Umino* [2010] refined the calibration of the log-based facies with data from the East Pacific Rise (EPR) and argued that the sequence from the sheeted dikes up to ~700 mbsf would be erupted on-axis and on the axial slope (within ~1 km of the axis, which equates to lithosphere formed within ~10 kyr for Site 1256). Further upward the stack consists of lava flows that traveled long distances (kilometers) from the ridge, sometimes ponding against impediments such as the normal faults that face toward the ridge axis (formed within ~20 kyr). The topmost lava pond would be an extreme example (suggested to be formed later, but not that much later).

The present magnetic-properties-based approach yields important information concerning the effects of alteration on a per sample basis. *Tominaga et al.*'s [2009] logging approach takes a different angle to the problem. The logs also collect information from brecciated and friable parts of the sequence that are undersampled by the drilling. Their calibration, however, requires core descriptions or a comparison to visible rocks elsewhere. On the other hand, rocks with similar porosity may have been altered to a variable extent. With the magnetic property analysis, this extent can be evaluated. Therefore, it is insightful to compare the two approaches.

The samples emerging as most pristine (ExPr cluster) on the basis of their magnetic properties are nearly always located above ~625 mbsf without a clear association to porosity (Figure 5). ExA samples in this segment are confined to the lava pond which is not amenable to electrofacies evaluation. It may indicate that exposure to higher temperature is a prime driver of thermochemical alteration in the partially maghemitized titanomagnetites. Below ~650 mbsf, a few scattered pristine samples occur. The zone where pillows and suspected pillows are identified in rather large abundance in the core descriptions and electrofacies analysis, and so in presumably dominantly porous rocks, is characterized primarily by samples from the ExA cluster. So, in addition to exposure to high temperature, prolonged exposure to hydrothermal fluid action has induced considerable alteration, which obscures the potential pristine character of the pillow lavas.

In general, ExPr samples have Curie temperatures below 350°C which is lower than the Curie temperature of the upper part of the lava stack in Hole 504B. In Hole 1256D, deeper ExPr samples have Curie temperatures up to ~400°C, which is distinctly high for "pristine" samples but in the range quoted for the upper portion of the lavas in Hole 504B [*Smith and Banerjee*, 1986]. One could anticipate the presence of some alteration in those samples, but not to a level sufficient to be classed in the ExA cluster (membership to the ExPr cluster is lower in those samples testifying to the gradual character of the alteration processes). In Hole 1256D, Curie temperatures are lower and more variable in the 250–700 mbsf interval than deeper downhole and in Hole 504B. The extrusive sequence is less hydrothermally altered than that of other basement sites, for instance Hole 504B [*Tominaga and Umino*, 2010]. This is in line with the lower T_C in Hole1265D relative to Hole 504B [*Smith and Banerjee*, 1986].

Below ~700 mbsf, Curie temperatures increase more slowly with depth than above [*Herrero-Bervera et al.*, 2011]. This could be tied to eruptive processes on the ridge axis that are characterized by a higher temperature regime than those slightly further away. Oxyexsolution occurs truly on axis to a higher degree leading to higher Curie temperatures [*Krása et al.*, 2011]. The more scattered nature of the Curie temperature distribution downhole in the 250–700 mbsf interval concurs with a more patchy nature of alteration compatible with deposition somewhat further away from the ridge axis. *Tominaga and Umino* [2010] infer a position on the axial slope between 1 and 2 km away from the ridge axis and further than 2 km away from the ridge axis for the extrusive sequence shallower than ~700 mbsf.

Below ~625 mbsf in the extrusive sequence, all samples are essentially allocated to the ExA and ExM clusters that express increasingly advanced alteration. Porosity seems less of an issue but it should be recalled that most extrusive rocks are rather porous by nature in comparison to intrusive rocks. Brecciation and fracturing of massive flows are described for this segment of the hole and supported by electrofacies data (Figure 5). The magnetic mineralogy enables one to discriminate between stages of alteration downhole. The more altered ExM samples primarily occur deeper than ~815 mbsf, in line with longer exposure to higher temperature. Samples from the lower half of the transition zone between the extrusive rocks and the sheeted dikes have magnetic properties (particularly T_C) similar to the dikes because they are thermally altered by the dikes. This behavior is similar to Hole 504B, where the extrusive sequence shows a gradual increase of T_C with depth and the upper part of the dikes have T_C of ~580°C indicating essentially unsubstituted magnetite. *Smith and Banerjee* [1986] interpreted the presence of submicroscopically exsolved titanomagnetite based on electron microprobe analysis.

The magnetic mineralogy of the dikes and gabbros has more structure and heterogeneity than evident from the electrofacies analysis (Figure 5). The varying size of intergrown magnetite lamellae in ilmenite and vice versa can be distinguished from their hysteresis properties; samples with the highest M_{rs}/M_s and lowest B_{cr}/B_c are expected to have smaller intergrowths than samples with lower M_{rs}/M_s and higher B_{cr}/B_c. The granoblastic portion of the sheeted dikes can clearly be distinguished based on its magnetic properties, as documented earlier. Thus, the magnetic approach reveals important information on the sheeted dikes interval of the hole.

The (isotropic) gabbro interval that is not amenable to investigation with logging tools appears to be magnetically highly variable. This hints at dynamic melt lens behavior (from which the dikes acted as feeders for the lavas) as a consequence of changes in magmastatic pressure [*France et al*., 2009]. Multiple intrusion events are likely to have occurred in Hole 1256D [*Koepke et al*., 2008] similar to the situation in a portion of the Southwest Indian Ridge where *Dick et al*. [2000] argued for multiple gabbro intrusion events. (Re)melting upon entrance of fluids in the hot base of the sheeted dikes as described for the Oman and Cyprus ophiolites [*Gillis and Roberts*, 1999; *Gillis*, 2002, 2008; *Gillis and Coogan*, 2002; *Coogan et al*., 2003; *Nicolas et al*., 2008] and for the Pito and Hess Deeps [*Gillis*, 2008] is argued to occur in Hole 1256D as well [*Wilson et al*., 2006; *Koepke et al*., 2008]. The sampled isotropic part of the gabbro would be a fossilized magma chamber, the foliated part of the gabbro has not (yet) been drilled in Hole 1256D.

6.3. Implications for Paleointensity Determination and the Expression of Magnetic Anomalies

In igneous rocks, the natural remanent magnetization (NRM) is considered to be acquired by cooling through the magnetic ordering or Curie temperature leading to a thermoremanent magnetization (TRM). However, many igneous rocks thermochemically alter during this cooling and ocean crust is not an exception. The alteration reactions are occurring, at least in part, below the magnetic minerals' Curie temperature resulting in a thermochemical remanent magnetization (TCRM). During the alteration process, the directional information of the NRM is preserved [e.g., *Matzka and Krása*, 2007; *Krása and Matzka*, 2007] although partial self-reversal has been observed [*Matzka et al*., 2003; *Doubrovine and Tarduno*, 2004]. The paleointensity record may be biased because of these TCRM processes [e.g., *Draeger et al*., 2006], although *Gee et al*. [2000] showed that the magnetic anomaly expression of the Brunhes Chron at the East Pacific Rise largely reflects paleointensity. Thus, at least for young fast spreading crust of the East Pacific Rise, acquisition of any subsequent CRM is relatively minor and occurs very shortly after the acquisition of the TRM. Therefore, the CRM will record the same geomagnetic field as the TRM, or will inherit the direction and part of the intensity of the original TRM.

Low-temperature oxidation of TM60 reduces its saturation magnetization and increases the Curie temperature [e.g., *O'Reilly*, 1984; *Xu et al*., 1996]. Prolonged low-temperature alteration of lava sequences has been argued to subdue the expression of magnetic anomalies up to ~20 Ma, followed by an increase up to ~120 Ma [*Bleil and Petersen*, 1983; *Furuta*, 1993; *Johnson and Pariso*, 1993; *Xu et al*., 1997; *Matzka et al*., 2003]. The composition and oxidation state of the titanomagnetite (in a broad sense) varies substantially on a local (centimeter) scale [e.g., *Gee and Kent*, 1998; *Xu et al*., 1997; *Zhou et al*., 2001]. *Xu et al*. [1997] suggest that preferential alteration of the finest particles is most important. However, in Hole 1256D *Krása et al*. [2011] show remarkably constant z values of ~0.6 (for large $>$ 10 μm grains) downhole over the entire extrusive sequence. They invoke spinodal exsolution into an increasingly Ti-poorer spinel phase and pseudobrookite, ilmenite, or anatase as the Ti-rich phase. This indicates that most alteration must have occurred relatively shortly after formation of the crust. Most metamorphism must occur rapidly when seen from a geological time perspective, since the crust is moving quickly away from the spreading ridge. For example, in the conceptual model of *Tominaga and Umino* [2010], the extrusive sequence of IODP Hole 1256D is constructed in ~30–50 kyr, which leaves little time for high-temperature metamorphic processes. A scenario to explain the results of *Gee et al*. [2000] could be that exsolution largely took place above the then prevailing Curie temperature thereby imprinting a relatively uncontaminated TRM on the rocks.

Temperature increases rapidly at the lava-dike transition since the dikes have a lower porosity (greenschist facies alteration throughout sheeted dike complex, e.g., *Mottl* [1983], *Bowers and Taylor* [1985], *Alt* [1995], *Gillis* [1995]). In the lowermost granoblastic dikes and gabbros below even higher temperatures have prevailed. The two-oxide geothermometer indicates temperatures of ~540–600°C for Hole 1256D gabbros [*Sauerzapf et al*., 2008]. This may imply that they provide a reasonably uncontaminated TRM upon cooling,

satisfying an important criterion for meaningful paleointensity (PI) experiments. Also *Pariso and Johnson* [1993] argue for a pure TRM in gabbros from ODP Site 735B because the magnetite formed during high-temperature alteration above its Curie temperature. However, the existence of intergrown lamellae in most of the dikes and gabbros in Hole 1256D casts doubt on the suitability of the magnetic grains for Thellier-style PI experiments. The potentially magnetically interacting lamellae makes the interpretation of other PI methods also cumbersome. *Herrero-Bervera and Acton* [2011] mention the possibility of retrieving PI values from glass, but that rarely occurs in Hole 1256D. Further the cooling time is poorly constrained, but is inevitably long (at least several tens of thousands of years because the dikes and gabbros in particular primarily cool conductively), thus integrating a comparatively long portion of geomagnetic field behavior. Thus, short-duration features of the geomagnetic field would not be resolvable.

The intensity of the NRM has direct bearing on the expression of the marine magnetic anomalies. The ridge axis central magnetic anomaly is prominent and requires high NRM intensities to explain the anomaly expression given the thin crust [e.g., *Harrison*, 1987]. The thickness of the source layer and its intensity cannot be solved simultaneously due to the inherent nonuniqueness of potential methods. Therefore, the locking-in profile of the NRM as function of depth is prescribed whereby sloping reversal boundaries are required to explain the skewness of the magnetic anomalies [e.g., *Kidd*, 1977; *Blakely and Lynn*, 1977]. *Tivey* [1996] could determine such sloping reversal boundaries along an escarpment at the Blanco fracture in the northeast Pacific Ocean. The NRM intensity in Hole 1256D (demagnetized at 25 mT to rule out drilling induced contributions) shows that the dikes are most strongly magnetized, about 3–5 times stronger than the majority of the extrusive segment above them [*Herrero-Bervera et al*., 2011]. The NRM-intensity of the gabbros is comparable to the extrusive rocks, so in line with conclusions by *Herrero-Bervera et al*. [2011] both dikes and gabbros contribute to the source layer of marine magnetic anomalies, at least for fast-spreading ocean crust.

Away from the ridge axis, flanking anomalies have a rapidly attenuating expression reaching a minimum in amplitude at ~20 Ma, while older anomalies slowly recover their amplitude. *Bleil and Petersen* [1983] attribute this behavior to ongoing progressive low temperature oxidation of the titanomagnetites in the extrusive rock pile. This lowers the NRM in intensity until a certain oxidation stage after which saturation magnetization increases again following the amplitude expression of the marine magnetic anomalies as function of distance to ridge axis. This TCRM acquisition has been adopted in subsequent models. *Masterton et al*. [2013] calculate a forward model for the remanent magnetization of the ocean crust taking the polarity timescale into account, retaining the CRM to TRM ratios and TRM decay times of *Raymond and Labrecque* [1987], and using the depth of 550°C Curie isotherm temperature following from the GDH1 plate model of *Stein and Stein* [1992]. By doing so, they could use a rather low but reasonably realistic initial TRM intensity of 0.5 A/m for the ocean crust in contrast to high values of 8.7 A/m required by *Raymond and Labrecque* [1987] for their 500 m thick layer responsible for the magnetic anomalies. The *Masterton et al*. [2013] forward model needs a considerable contribution from induced magnetization to match with observations from the satellite-observations-based MF7 model.

The above calculation applies a magnetite Curie isotherm of 550°C, which is appropriate for sheeted dikes and gabbro but not for the extrusive sequence. The latter has Curie temperatures 150–250°C in the top part and rising to 400–450°C just before the sheeted dikes. The rise in Curie temperature is the consequence of spinodal exsolution during prolonged exposure to very low-grade metamorphic temperatures [*Krása et al*., 2011]. This would imply that the lower portion of the extrusive sequence acquires its T(C)RM after having been cooled below this temperature, further away from the ridge at a later time than the sheeted dikes and gabbros.

Further it should be recalled that magnetization and remanences are distinctly temperature-dependent, much more than the low-field susceptibility responsible for the induced magnetization. So, the same rock containing (titano)magnetite has a lower remanence closer to its magnetic ordering or Curie temperature with the concomitant reduced expression of its magnetic anomaly. Thus, in addition to larger distance, the higher temperature of the deeper rocks also contributes to a weaker remanence. However, with time the ocean crust cools. Hence, the older the ocean crust, the thicker the rock with temperatures below the Curie isotherm, and the higher the remanence contribution of deep seated rocks. Close to the ridge axis, the isotherms are near vertical but the planes of equal temperature become increasingly horizontal further away. The result is a stack of normal and reversed polarity zones with the youngest zone (Brunhes Chron) deepest,

which should have no influence on marine magnetic anomalies when the contributions of normal and reversed parts compensate each other. In addition to the cumulative normal and reversed chron duration, the temperature distribution in the ocean crust is also important. Short-duration chrons will have a small effect because of viscous resetting that is more prominent at high temperatures. In principle, normal and reversed zones of equal duration would cancel out; however, upon further cooling temperature differences between more shallow and deeper seated sources may lead to a contribution to the measured magnetic anomaly.

7. Conclusions

Cluster analysis enables the identification of groups within which the oceanic crustal rocks have common rock magnetic properties owing to different magmatic processes and degrees of hydrothermal alteration. Relatively pristine samples identified only in the top half of the extrusive section may contain a reasonably uncontaminated TRM if alteration occurs near or at the ridge axis while the extrusive unit is still above the Curie temperature of the constituent titanomagnetite grains. This would enable retrieval of a meaningful absolute paleointensity from such levels. Altered and relatively fine-grained extrusives and slightly more altered multidomain extrusives, both of which have higher Curie temperatures than the pristine extrusives, dominate the lower half of the extrusive section and contain a TCRM. Magnetic properties similar to the more altered extrusives also occur in some of the gabbros that have been affected by granoblastic metamorphism [*Koepke et al*., 2008]. The remaining part of the gabbroic section and the lowermost dikes contain (nearly) pure magnetite that has an uncontaminated TRM because alteration occurred above the Curie temperature of magnetite, allowing in principle for paleointensity determination. However, cooling times may be long so that short-duration geomagnetic events cannot be resolved. The entire drilled sequence can retain a stable natural remanent magnetization and as such contributes to the expression of marine magnetic anomalies.

As noted before by several workers [e.g., *Tominaga et al*., 2009], massive and nonfragile lithologies are probably overrepresented in recovered core material since brecciated and fragmented material is crushed and lost during the drilling process. Hence, seawater-basalt interaction may be underestimated. The present cluster analysis (of course under the proviso of available core material) shows that the massive and the fractured massive flows may also be altered, particularly in the deeper portion of the extrusive lava pile. Further refinement to the cluster analysis should be possible with additional rock magnetic data such as the frequency dependence of susceptibility, ARM intensity, the susceptibility of the ARM, and possibly σ_{hys} and/or other parameters proposed by *Fabian* [2003].

The on-axis and slightly off-axis crustal construction as proposed by *Tominaga and Umino* [2010] based on electrofacies analysis and core descriptions is fully supported by the present cluster analysis. Both approaches, cluster analysis of magnetic properties and log-based electrofacies analysis, appear to complement each other. While porosity differences can be visualized with electrofacies analysis, thermochemical alteration of titanomagnetites is also the result of prolonged exposure to elevated temperatures. Furthermore, it enables a refined characterization of the nonporous parts of the ocean crust. As such, it delivers important additional information pertaining to Hole 1256D, on the lava pond interval, the gabbro interval, and it provides a structured picture of the sheeted dikes including its granoblastic overprinted lowermost part.

Acknowledgments

This research used samples and data provided by the Ocean Drilling Program (ODP) and the Integrated Ocean Drilling Program (IODP). We give special thanks to the participating scientists and crew members of JOIDES Resolution for their help and support during the scientific cruises. Tilo von Dobeneck and an anonymous reviewer are thanked for their constructive comments that were helpful in improving this contribution. Funding for this research was provided by the National Science Foundation (NSF) through its support of ODP, IODP, and the United States Science Support Program (USSSP) and through NSF grants JOI-T309A4, OCE-0727764, and EAR-IF-0710571 to E.H.-B., a USSSP Post-Expedition Activity Award and NSF grant OCE-0727576 to Acton. Additional financial support to E.H.-B. was provided by SOEST-HIGP. This is an HIGP and SOEST contribution 2046 and 9184, respectively. D.H. was supported as part of an Australian Research Council Discovery Project (grant DP110105419). D.K. was funded by a Royal Society of Edinburgh BP Trust Research Fellowship. M.J.D. acknowledges support during his sabbatical stays in Honolulu and Canberra. The views expressed are purely those of the authors and may not in any circumstances be regarded as stating an official position of the European Research Council Executive Agency.

References

Abonyi, J., and R. Babuska (2004), FUZZSAM: Visualization of fuzzy clustering results by modified Sammon mapping, paper presented at Proceedings of 2004 IEEE International Conference on Fuzzy Systems, 2004, pp. 365–370, IEEE, N. Y., doi:10.1109/FUZZY.2004.1375750. [Available at http://ieeexplore.ieee.org/stamp/stamp.jsp?arnumber=1375750.]

Alt, J.C. (1995), Sulfur isotopic profile through the oceanic crust: Sulfur mobility and seawater-crustal sulfur exchange during hydrothermal alteration, *Geology*, *23*, 585–588.

Andersen, D. J., D. H. Lindsley, and P. M. Davidson (1993), QUILF: A Pascal program to assess equilibria among Fe-Mg-Mn-Ti oxides, pyroxenes, olivine, and quartz, *Comput. Geosci.*, *19*, 1333–1350, doi:10.1016/0098-3004(93)90033-2.

Bezdek, J. C. (1974), Cluster validity with fuzzy sets, *J. Cybern.*, *3*, 58–73.

Bezdek, J. C. (1992), Computing with uncertainty, *IEEE Commun. Mag.*, *30*, 24–36.

Bezdek, J. C., R. Erhlich, and W. Full (1984), FCM: The fuzzy c-means clustering algorithm, *Comput. Geosci.*, *10*, 191–203.

Blakely, R. J. (1995), *Potential Theory in Gravity and Magnetic Applications*, Cambridge Univ. Press, Cambridge, U. K.

Blakely, R. J., and W. S. Lynn (1977), Reversal transition widths and fast-spreading centers, *Earth Planet. Sci. Lett.*, *33*, 321–330.

Bleil, U., and N. Petersen (1983), Variations in magnetization intensity and low temperature titanomagnetite oxidation of ocean floor basalts, *Nature*, *301*, 384–388.
Bowers, T. S., and H. P. Taylor Jr. (1985), An integrated chemical and stable-isotope model of the origin of mid-ocean ridge hot spring systems, *J. Geophys. Res.*, *90*, 12,583–12,606.
Burrough, P. A., P. F. M. van Gaans, and R. J. Hootsmans (1997), Continuous classification in soil survey: Spatial correlation, confusion and boundaries, *Geoderma*, *77*, 115–135.
Burrough, P. A., P. F. M. van Gaans, and R. MacMillan (2000), High-resolution landform classification using fuzzy k-means, *Fuzzy Sets Syst.*, *113*, 37–52.
Coogan, L. A., N. C. Mitchell, and M. J. O'Hara (2003), Roof assimilation at fast spreading ridges: An investigation combining geophysical, geochemical, and field evidence, *J. Geophys. Res.*, *108*(B1), 2002, doi:10.1029/2001JB001171.
Dave, R. N. (1996), Validating fuzzy partition obtained through c-shells clustering, *Pattern Recogn.*, *17*, 613–623.
Day, R., M. D. Fuller, and V. A. Schmidt (1977), Hysteresis properties of titanomagnetites: Grain size and composition dependence, *Phys. Earth Planet. Inter.*, *13*, 260–267.
Dekkers, M. J., C. G. Langereis, S. P. Vriend, P. J. M. van Santvoort, and G. J. de Lange (1994), Fuzzy c-means cluster analysis of early diagenetic effects on natural remanent magnetisation acquisition in a 1.1 Myr piston core from the Central Mediterranean, *Phys. Earth Planet Inter.*, *85*, 155–171.
Dick, H. J. B., et al. (2000), A long in situ section of the lower ocean crust: Results of ODP Leg 176 drilling at the Southwest Indian ridge, *Earth Planet. Sci. Lett.*, *179*, 31–51.
Doubrovine, P. V., and J. A. Tarduno (2004), Self-reversed magnetization carried by titanomaghemite in oceanic basalts, *Earth Planet. Sci. Lett.*, *222*, 959–969.
Draeger, U., M. Prévot, T. Poidras, and J. Riisager (2006), Single-domain chemical, thermochemical and thermal remanences in a basaltic rock, *Geophys. J. Int.*, *166*, 12–32.
Dunlop, D. J. (2002), Theory and application of the Day plot (M_{rs}/M_s versus H_{cr}/H_c) 1. Theoretical curves and tests using titanomagnetite data, *J. Geophys. Res.*, *107*(B3), 2056, doi:10.1029/2001JB000486.
Dziony, W., J. Koepke, and F. Holtz (2008), Data report: Petrography and phase analyses in lavas and dikes from the hole 1256D (ODP Leg 206 and IODP Expedition 309, East Pacific Rise), in *Proceedings of the Integrated Ocean Drilling Program*, vol. 309/312, 22 pp., Integr. Ocean Drill. Program Manage. Int. Inc., Washington, D. C. doi:10.2204/iodp.proc.309312.201.2008. [Available at http://publications.iodp.org/proceedings/309_312/201/201_.htm.]
Fabian K. (2003), Some additional parameters to estimate domain state from isothermal magnetization measurements, *Earth Planet. Sci. Lett.*, *213*, 337–345.
France, L., B. Ildefonse, and J. Koepke (2009), Interactions between magma and hydrothermal system in Oman ophiolite and in IODP Hole 1256D: Fossilization of a dynamic melt lens at fast spreading ridges, *Geochem. Geophys. Geosyst.*, *10*, Q10O19, doi:10.1029/2009GC002652.
Francheteau, J., R. Armijo, J. L. Cheminee, R. Hekinian, P. Lonsdale, and N. Blum (1990), 1 Ma East Pacific Rise oceanic crust and uppermost mantle exposed by rifting in Hess Deep (equatorial Pacific Ocean), *Earth Planet. Sci. Lett.*, *101*, 281–295.
Furuta, T. (1993), Magnetic properties and ferromagnetic mineralogy of oceanic basalts, *Geophys. J. Int.*, *113*, 95–114.
Gee, J., and D. V. Kent (1998), Magnetic telechemistry and magmatic segmentation on the southern East Pacific Rise, *Earth Planet. Sci. Lett.*, *164*, 379–385.
Gee, J. S., and D. V. Kent, (2007), Source of oceanic magnetic anomalies and the geomagnetic polarity timescale, In *Treatise on Geophysics*, vol. 5, *Geomagnetism*, edited by M. Kono, pp. 455–507, Elsevier, Amsterdam.
Gee, J. S., S. C. Cande, J. A. Hildebrand, K. Donnelly, and R. L. Parker (2000), Geomagnetic intensity variations over the past 780 kyr obtained from near-seafloor magnetic anomalies, *Nature*, *408*, 827–832.
Gillis, K. M. (1995), Controls on hydrothermal alteration in a section of fast-spreading oceanic crust, *Earth Planet. Sci. Lett.*, *134*, 473–489.
Gillis, K. M. (2002), The root zone of an ancient hydrothermal system exposed in the Troodos ophiolite, *Cyprus. J. Geol.*, *110*, 57–74, doi:10.1086/324205.
Gillis, K. M. (2008), The roof of an axial magma chamber: A hornfelsic heat exchanger, *Geology*, *36*, 299–302, doi:10.1130/G24590A.1.
Gillis, K. M., and L. A. Coogan (2002), Anatectic migmatites from the roof of an ocean ridge magma chamber, *J. Petrol.*, *43*, 2075–2095, doi:10.1093/petrology/43.11.2075.
Gillis, K. M., and M. D. Roberts (1999), Cracking at the magma-hydrothermal transition: Evidence from the Troodos ophiolite, *Cyprus. Earth Planet. Sci. Lett.*, *169*, 227–244.
Hanesch, M., R. Scholger, and M. J. Dekkers (2001), The application of fuzzy c-means cluster analysis and non-linear mapping to a soil data set for the detection of polluted sites, *Phys. Chem. Earth A*, *26*, 885–891.
Harrison, C. G. A. (1987), Marine magnetic anomalies: The origin of the stripes, *Annu. Rev. Earth Planet. Sci.*, *15*, 505–543.
Herrero-Bervera, E., and G. Acton (2011), Absolute Paleointensities From an Intact Section of Oceanic Crust Cored at ODP/IODP Site 1256 in the Equatorial Pacific, The Earth's magnetic interior, *IAGA Spec. Sopron Book Ser. 1*, Springer, Heidelberg, Berlin, doi:10.1007/978-94-007-0323-0_13.
Herrero-Bervera, E., D. Krasa, G. Acton, S. Rodriguez Durand, and M. J. Dekkers (2011), Rock magnetic characterization through an intact sequence of oceanic crust, IODP Hole 1256D, The Earth's magnetic interior, *IAGA Spec. Sopron Book Ser. 1*, Springer doi:10.1007/978-94-007-0323-0_11.
Holland, T., and J. Blundy (1994), Non-ideal interactions in calcic amphiboles and their bearing on amphibole-plagioclase thermometry, *Contrib. Mineral. Petrol.*, *116*, 433–447, doi:10.1007/BF00310910.
Höppner, F., F. Klawonn, F. Kruse, and T. Runkler (1999), *Fuzzy Cluster Analysis*, John Wiley, Chichester, U. K.
Johnson, H. P., and J. E. Pariso (1993), Variations in oceanic crustal magnetization: Systematic changes in the last 160 million years, *J. Geophys. Res.*, *98*, 435–445.
Kidd, R. G. W. (1977), The nature and shape of the sources of marine magnetic anomalies, *Earth Planet. Sci. Lett.*, *33*, 310–320.
Koepke J., D. M. Christie, W. Dziony, F. Holtz, D. Lattard, J. Maclennan, S. Park, B. Scheibner, T. Yamasaki, and S. Yamazaki (2008), Petrography of the dike-gabbro transition at IODP Site 1256 (equatorial Pacific): The evolution of the granoblastic dikes, *Geochem. Geophys. Geosyst.*, *9*, Q07O09, doi:10.1029/2008GC001939.
Krása, D., and J. Matzka, (2007), Inversion of titanomaghemite in oceanic basalt during heating, *Phys. Earth Planet. Inter.*, *160*, 169–179.
Krása, D., E. Herrero-Bervera, G. Acton, and S. Rodriguez (2011), Magnetic mineralogy of a complete oceanic crustal section (IODP Hole 1256D), The Earth's magnetic interior, *IAGA Spec. Sopron Book Ser. 1*, Springer, Heidelberg, Berlin, doi:10.1007/978-94-007-0323-0_12.

Lamoureux, G., B. Ildefonse, and D. Mainprice (1999), Modelling the seismic properties of fast-spreading ridge crustal low-velocity zones: Insights from Oman gabbro textures, *Tectonophysics*, *312*, 283–301, doi:10.1016/S0040-1951(99)00183-3.
Lattard, D., R. Engelmann, A. Kontny, and U. Sauerzapf (2006), Curie temperatures of synthetic titanomagnetites in the Fe-Ti-O system: Effects of composition, crystal chemistry, and thermomagnetic methods, *J. Geophys. Res.*, *111*, B12S28, doi:10.1029/2006JB004591.
Lucieer, V., and A. Lucieer (2009), Fuzzy clustering for seafloor classification, *Mar. Geol.*, *264*, 230–241, doi:10.1016/j.margeo.2009.06.006.
Masterton, S. M., D. Gubbins, R. D. Müller, and K. H. Singh (2013), Forward modeling of oceanic lithospheric magnetization, *Geophys. J. Int.*, *192*, 951–962.
Matzka, J., and D. Krása (2007), Oceanic basalt continuous thermal demagnetization curves, *Geophys. J. Int.*, *169*, 941–950.
Matzka, J., D. Krasa, T. Kunzmann, A. Schult, and N. Petersen (2003), Magnetic state of 10–40Ma old ocean basalts and its implications for natural remanent magnetization, *Earth Planet. Sci. Lett.*, *206*, 541–553.
Mottl, M. J. (1983), Metabasalts, axial hot springs, and the structure of hydrothermal systems at mid-ocean ridges, *Geol. Soc. Am. Bull.*, *94*, 161–180.
Nicolas, A., F. Boudier, J. Koepke, L. France, B. Ildefonse, and C. Mevel (2008), Root zone of the sheeted dike complex in the Oman ophiolite, *Geochem. Geophys. Geosyst.*, *9*, Q05001, doi:10.1029/2007GC001918.
O'Reilly, W. (1984), *Rock and Mineral Magnetism*, 220 pp, Chapman and Hall, New York, N. Y.
Pakhira, M. K., S. Bandyopadhyay, and U. Maulik, (2005), A study of some fuzzy cluster validity indices, genetic clustering and application to pixel classification, *Fuzzy Sets Syst.*, *155*, 191–214.
Pariso, J. E., and H. P. Johnson (1993), Do lower crustal rocks record reversals of the earth's magnetic field?: Magnetic petrology of oceanic gabbros from Ocean Drilling Program Hole 735B, *J. Geophys. Res.*, *98*, 16,013–16,032.
Phipps Morgan, J., and Y. J. Chen (1993), The genesis of oceanic crust: Magma injection, hydrothermal circulation, and crustal flow, *J. Geophys. Res.*, *98*, 6283–6297.
Raymond, C. A., and J. L. Labrecque (1987), Magnetization of the oceanic crust: Thermoremanent magnetization or chemical remanent magnetization?, *J. Geophys. Res.*, *92*, 8077–8088.
Sammon, J. W. (1969), A non-linear mapping for data structure analysis, *IEEE Trans. Comput.*, *C18*, 401–409.
Sauerzapf, U., D. Lattard, M. Burchard, and R. Engelmann (2008), The titanomagnetite-ilmenite equilibrium: New experimental data and thermo-oxybarometric application to the crystallization of basic to intermediate rocks, *J. Petrol.*, *49*, 1161–1185, doi:10.1093/petrology/egn021.
Schmidt A. M., T. von Dobeneck, and U. Bleil (1999), Magnetic characterization of Holocene sedimentation in the South Atlantic, *Paleoceanography*, *14*, 465–481.
Smith, G. M., and S. K. Banerjee (1986), Magnetic structure of the upper kilometer of the marine crust at Deep Sea Drilling Project Hole 504B, Eastern Pacific Ocean, *J. Geophys. Res.*, *91*, 10337–10354.
Stein, C. A., and S. Stein (1992), A model for the global variation in oceanic depth and heat flow with lithospheric age, *Nature*, *359*, 123–129.
Suhr, G., E. Hellebrand, K. Johnson, and D. Brunelli (2008), Stacked gabbro units and intervening mantle: A detailed look at a section of IODP Leg 305, Hole U1309D, *Geochem. Geophys. Geosyst.*, *9*, Q10007, doi:10.1029/2008GC002012.
Tartarotti, P., E. Fontana, and L. Crispini (2009), Deformation pattern in a massive ponded lava flow at ODP-IODP Site 1256: A core and log approach, *Geochem. Geophys. Geosyst.*, *10*, Q05O17, doi:10.1029/2008GC002346.
Teagle, D. A. H., J. C. Alt, S. Umino, S. Miyashita, N. R. Banerjee, D. S. Wilson, and Shipboard Scientists (2006), In *Proceedings of the Integrated Ocean Drilling Program*, vol. 309/312, Integr. Ocean Drill. Program Manage. Int., Inc., Washington, D. C.
Tivey, M. A. (1996), Vertical magnetic structure of ocean crust determined from near-bottom magnetic field measurements, *J. Geophys. Res.*, *101*, 20275–20296.
Tominaga, M., and S. Umino (2010), Lava deposition history in ODP Hole 1256D: Insights from log-based volcanostratigraphy, *Geochem. Geophys. Geosyst.*, *11*, Q05003, doi:10.1029/2009GC002933.
Tominaga, M., D. A. H. Teagle, J. C. Alt, and S. Umino (2009), Determination of the volcanostratigraphy of ocean crust formed at superfast spreading ridge: Electrofacies analyses of ODP/IODP Hole 1256D, *Geochem. Geophys. Geosyst.*, *10*, Q01003, doi:10.1029/2008GC002143.
Torres, G. J., R. B. Basnet, A. H. Sung, S. Mukkamala, and B. M. Ribeiro (2008), A similarity measure for clusters and its applications, in *Proceedings of World Academy of Science, Engineering and Technology*, vol. 31, pp. 490–496, World Academy of Science, Vienna, Austria. [Available at https://www.cs.nmt.edu/~rbasnet/research/ClusteringSimilarityAndItsApplications.pdf.].
Vlag, P. A., P. P. Kruiver, and M. J. Dekkers (2004), Evaluating climate change by multivariate statistical techniques on magnetic and chemical properties of marine sediments (Azores region). *Palaeogeogr. Palaeoclimatol. Palaeoecol.*, *212*, 23–44.
Vriend, S. P., P. F. M. van Gaans, J. Middelburg, and A. de Nijs (1988), The application of fuzzy c-means cluster analysis and non-linear mapping to geochemical datasets: examples from Portugal, *Appl. Geochem.*, *3*, 213–224.
Wilson, D. S., et al. (2003), Proc. Ocean Drill. Program, Init. Repts., 206, College Station, Tex., doi:10.2973/odp.proc.ir.206.2003.
Wilson, D. S., et al. (2006), Drilling to gabbro in intact ocean crust, *Science*, *312*, 1016–1020, doi:10.1029/2008GC002143.
Wu, K. L., and M. Yang (2005), A cluster validity index for fuzzy clustering, *Pattern Recogn. Lett.*, *26*, 1275–1291.
Xie, X. L., and G. Beni, (1991), A validity measure for fuzzy clustering, *IEEE Trans. Pattern Anal.*, *13*, 841–847.
Xu, W., D. Peacor, R. Van der Voo, W. Dollase, and R. T. Beaubouef (1996), Modified lattice parameter/Curie temperature diagrams for titanomagnetite/titanomaghemite within the quadrilateral Fe_3O_4 - Fe_2TiO_4 - Fe_2O_3 - Fe_2TiO_5, *Geophys. Res. Lett.*, *23*, 2811–2814, doi:10.1029/96GL01117.
Xu, W., R. Van der Voo, D. R. Peacor, and R. T. Beaubouef (1997), Alteration and dissolution of fine-grained magnetite and its effects on magnetization of the ocean floor, *Earth Planet. Sci. Lett.*, *151*, 279–288.
Zhou, W., R. Van der Voo, D. R. Peacor, D. Wang, and Y. Zhang (2001), Low-temperature oxidation in MORB of titanomagnetite to titanomaghemite: A gradual process with implications for marine magnetic anomaly amplitudes, *J. Geophys. Res.*, *106*, 6409–6421.